Computational Materials Science 127 (2017) 194–203

Contents lists available at ScienceDirect

Computational Materials Science

journal homepage: www.elsevier.com/locate/commatsci

Deformation mechanisms in nanoporous metals: Effect of ligament shape and disorder

J. Jiao [a,*], N. Huber [a,b]

[a] Institute of Materials Research, Materials Mechanics, Helmholtz-Zentrum Geesthacht, Germany
[b] Institute of Materials Physics and Technology, Hamburg University of Technology, Germany

ARTICLE INFO

Article history:
Received 29 August 2016
Received in revised form 24 October 2016
Accepted 29 October 2016
Available online 16 November 2016

Keywords:
Nanoporous gold
Mechanical behavior
Ligament shape
Randomization
Deformation mechanisms

ABSTRACT

The current work presents a numerical modelling approach for investigating the effect of ligament shape and disorder on the macroscopic mechanical response of nanoporous gold (NPG). The approach starts from a 'single ligament' analysis with respect to three fundamental deformation modes, bending, torsion, and compression, that depend on the ligament shape. It can be shown that the predictive capability of the highly computationally efficient beam model is sufficient for a large variation in ligament shapes. Using a representative volume element (RVE) composed of such ligaments, different degrees of disorder are included. For both the single ligament and RVE models, the cylindrical beam serves as a common reference to compare the results when varying the ligament shape. From the comparison of the RVE elastic response with the single ligament results and the further analysis of statistical information from the elements in the RVE, it is found that bending is the major deformation mode for perfectly ordered RVEs, whereas torsion gains importance for increasing RVE disorder. The effect of compression of the ligaments can be neglected in general. It is concluded that the transition to torsion deformation due to disorder is the cause of the strongly reduced lateral expansion during compression deformation of NPG.

1. Introduction

Nanoporous gold (NPG) made by de-alloying can be produced as macroscopic objects that exhibit a bi-continuous network of nanoscale pores and solid 'ligaments' [1]. The solid fraction of the porous body is approximately 30% [1,2]. Recent studies explored the use of NP metals, especially NPG, made by de-alloying as a functional material for catalysis, actuation and sensing [3–5]. Mechanical performance is relevant to each of these fields. It is therefore necessary to gain a fundamental understanding of the mechanical behavior of such a material. Experimental tests on the compression, tension, fracture, and indentation of NPG reflect the current interest in this material [6,7]. Numerous experimental studies reported that in addition to the relative density, the strength of NPG strongly depends on its average ligament radius [8–10], that is, the macroscopic strength of NPG increases with decreasing ligament size [2,11–14].

There is no doubt that one of the most interesting features that NPG materials possess is the famous 'size effect' [9,14], i.e., different macroscopic mechanical responses have been observed for different ligament sizes, specifically different ligament radii, for the same solid fraction. However, the fundamental reason for this effect is still under debate.

It would be rational to state that the macroscopic mechanical response of an NPG material is mostly influenced by two aspects: the constitutive material law and the geometrical/structural properties of the ligament network. Concerning the constitutive law, extensions to classical continuum plasticity models, e.g., as applied in [7,15], have been suggested for including size effects by splitting the volume and the surface into separate models [16] or in the form of a gradient extended crystal plasticity theory [17]. In this way, a size-dependent elastic modulus or size-dependent plasticity can be predicted. The latter is computationally expensive, so until now, relatively simple honeycomb-like 2D-structures have been studied.

Choosing an arbitrary average ligament size, the size effect reduces to a given Young's modulus and yield strength captured with the material parameters of a conventional plasticity model. Microscopic features such as surface effects are ignored. In this way, attention is drawn towards the influence of the shape-related parameters of NP materials as has been analyzed previously in several works [7,15,18–21]. One could argue that the determination of the size effect for NP materials, typically making

* Corresponding author.
E-mail address: jingsi.jiao@hzg.de (J. Jiao).

http://dx.doi.org/10.1016/j.commatsci.2016.10.035
0927-0256/

use of models translating macroscopic stress into local stresses acting in the ligaments, requires the knowledge of the relationship between the shape-related properties and the macroscopic mechanical response.

Motivated by previous publications [7,15,18–21], where all ligaments were assumed to be cylindrical and of the same size, Pia and Delogu [18] conducted a statistical analysis for quadratic beams, focusing on the relationship between the morphological features of the ligaments and the mechanical responses of the NP materials. In their study, a simplified polynomial equation (Eq. (1)) was applied to describe the geometrical profiles of different ligament variations extracted from scanning electron microscopy (SEM) micrographs. Based on these statistical morphology data, a phenomenological model based on Timoshenko's beam bending theory was developed to describe elastic bending. Their work brought further insight towards revealing the influences on the elastic response produced by the ligament geometry of NP materials.

$$r = nx^2 + m \tag{1}$$

In Eq. (1), r denotes the ligament radius and x is the axial coordinate with $x = 0$ being the ligament's center. The shape of the ligament is defined as $n = (r_{end} - r_{mid})/(l/2)^2$ and $m = r_{mid}$, where, r_{end} is the radius at the ends, r_{mid} is the radius in the middle of the ligament, and l is the length of the ligament.

When considering the work of Pia and Delogu [18] as an important element describing the relationship between the ligament geometrical properties and the macroscopic mechanical response, another equally important element to consider is the network construction of the NP materials. Based on the 'ball-and-stick' beam model proposed by Huber et al. [7], Roschning and Huber [15] conducted a thorough investigation on the influences of the randomization parameter (A) of network randomization on the mechanical response of an RVE. It was found that the Young's modulus (E), yield strength (σ_y), and elastic Poisson's ratio (ν_E) are heavily influenced by A. This is mainly because A, as the major structural parameter across the whole RVE, is responsible for describing the length variation and curvatures of the ligaments that control the deformation mechanisms within the ligament network.

The works of [7,15,18] were the pioneering efforts for analytically characterizing the effects of the geometrical and structural properties of NP materials on the mechanical responses of NP materials. This inspired a further study combining both approaches into one comprehensive work. It is worthwhile to note that most of the work studying the mechanical behavior of NP metals is based on macroscopic compression. Samples can be produced in mm to cm scale in a quality allowing large plastic deformation in such tests [22]. It has been assumed in [7,18,19,23] that during macroscopic compression, bending is the dominant deformation mechanism and that the effects of axial tension and compression within the ligaments can be neglected.

NP materials show immediate brittle failure in experiments under macroscopic tension. So far, the only way to prevent this is by infiltration with a polymer. It has been shown recently that such a material can be deformed in four-point bending to considerable strains [24]. However, there exist theoretical studies, such as [25], that investigated the scaling laws of an NPG under macroscopic tension. In addition, in the MD simulations presented in [25], progressive necking and rupture were observed, but the stress-strain data before that point could be used to fit the Gibson-Ashby model. The resulting scaling law contains an additional term, which is linear for the Young's modulus. This underlines the relevance of tension deformation within the ligaments, which reflects the increasing alignment of the ligaments during macroscopic tensile deformation.

The present work establishes the relationship between the geometrical and structural properties and the corresponding mechanical responses, beginning with the analysis of single ligaments. The ligaments serve as building blocks with variable geometrical properties defined by a few parameters. In an extension to [18], the mechanical response is investigated not only for bending but also for three fundamental loading cases, i.e., bending, torsion, and compression, depending on the geometrical parameters. This is followed by analyses of compressing ordered and disordered NPG networks composed of a large number of such ligaments within an RVE with regard to the elastic modulus and yield strength. This brings the discussion to the structural level, following [7,15]. A close correlation between the single ligament geometry and the macroscopic mechanical response of the RVE is revealed, and the contributions from bending, torsion, and compression on the deformation mechanisms are discussed.

2. Single ligament analysis

2.1. Model setup

2.1.1. Geometry determination

The finite element analysis (FEA) code ABAQUS/Implicit [26] is used for this analysis. Both beam and solid elements are applied for the single ligament analysis. The objective of applying a computationally more expensive solid model is to examine the applicability and accuracy of the beam model that offers excellent computational efficiency for a spectrum of typical ligament geometries and loading conditions. In the following, r and l denote ligament radius and ligament length, respectively, as illustrated in Fig. 1a. According to Eq. (1), the ligament radius of the cylindrical ligament is denoted as $r(n = 0) = r_0$, and the aspect ratio of a ligament is defined as r_0/l, i.e., the cylindrical ligament serves as a common reference for all ligament geometries throughout this work.

A shear deformable beam element has been compared with a solid element using a Kalvin unit cell [27], validating the modelling capability of the beam element for open cell foam structures with a solid fraction φ ranging from 2% to 9% for polyester urethane and aluminum foams. However, unlike the thin beam with a small aspect ratio $r_0/l \approx 0.1$ as used in [27], ligaments with a larger r_0/l ratio of approximately 0.25 are typical for NPG materials [7,15]. This leads to the question of whether the beam element is capable of capturing the main characteristics of the thick ligaments with sufficient accuracy, i.e., deviations should be below the uncertainties in the experiments on NPG.

Fig. 1b shows that the ligament shape varies significantly in a real material. To analytically describe the ligament shapes, a quadratic equation (Eq. (1)) is implemented, following Pia and Delogu [18]. Ligaments with varying shapes can be characterized using the dimensionless parameter $n \cdot r_0$. For $n \cdot r_0 > 0$, the ligament shape is concave, while for $n \cdot r_0 < 0$, the ligament has a convex shape. While [18–20] exclusively studied the case of $n \cdot r_0 > 0$, the geometries found in [28] by analyzing the 3D FIB tomography of polymer-infiltrated NPG suggests extending the analysis to $n \cdot r_0 < 0$. Such convex ligaments are supposed to originate from the pinching-off and retracting of ligaments during heat treatment and coarsening, leaving a mass concentration, also called a "dangling" ligament.

The solid fraction φ is the major parameter for describing the structure-property relationship of NP materials [2,29]. The calculation of φ for RVE in the current paper can be found in [15], which is derived from the ball-stick model of the diamond

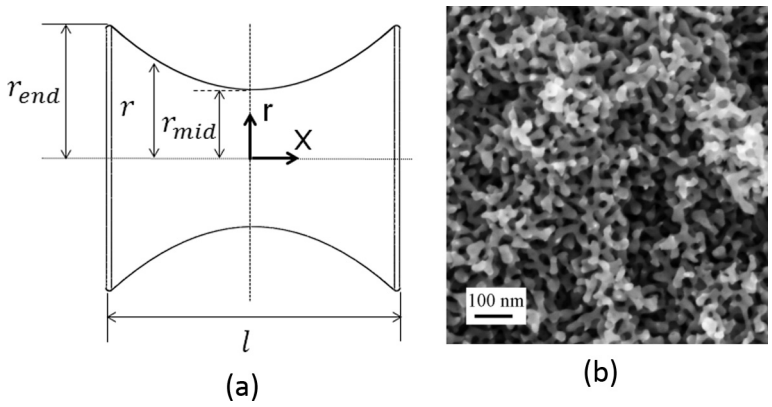

Fig. 1. (a) Schematic of the ligament shape, characterized by the ratio r_{mid}/r_{end}; (b) SEM of the surface of an NPG sample [30].

unit cell structure proposed in [7]. In the following study, a constant material volume is assigned to all the ligaments of different shapes to eliminate the influence of the solid fraction. Therefore, the ligament shape is the only variable in the analysis. In the current section, the ligament material volume is chosen as equal to the volume of the cylindrical ligament of $r_0/l = 0.25$ that is statistically close to the aspect ratio found in the NPG studies of [7,15]. The relation can be described with Eq. (2), where m ($= r_{mid}$) can be determined for given values of n and r_0 according to Eq. (3). The shape representative ratio r_{mid}/r_{end} used in the rest of the paper, as illustrated in Fig. 1a, can be calculated by combining Eq. (3) and Eq. (1).

$$\pi r_0^2 L = \pi \int_{-l/2}^{l/2} (nx^2 + m)^2 dx \tag{2}$$

$$m = -\frac{l^2 n}{12} + \sqrt{r_0^2 - \frac{l^4 n^2}{180}} \tag{3}$$

For the beam model, different radii of sections were assigned to the elements along an entire ligament consisting of 20 elements (B31), which is schematically illustrated in Fig. 2a. A sketch of the solid element geometry (C3D8R) model is shown in Fig. 2b, presenting the same geometry. The solid model is uniformly meshed with approximately 60,000 elements. Its accuracy is ensured by a mesh convergence check.

2.1.2. Loading and boundary conditions

To analytically dissect the complex loading condition of the ligaments, which appears during compression of a real NPG material, three fundamental loading conditions are separately analyzed, which are bending, torsion, and compression. As shown in Fig. 2, only half of the ligament is modelled to reduce the computational cost. The load is applied in the center of the ligament, while the other end of the ligament, which would connect to other ligaments in a node of an NPG network, is fixed by the boundary conditions. The load is applied in the form of displacements (w for bending and v for compression) and rotation (θ for torsion), as shown in Fig. 2. This approach is feasible because until the onset of plastic yielding, all three deformation modes can be superimposed due to the linearity of the elasticity.

To apply the same loading condition to the solid model as to the beam model, the symmetry surface is coupled to a rigid plate a 'Coupling' constraint that has a 'Continuum distribution' [26], as shown in Fig. 2b. The loading can therefore be assigned to the center point of the rigid plate and distributed to the whole surface [26]. This approach ensures the maximum level of the similarity between the solid and beam models with respect to the load application. An elastic-perfectly plastic material model of the bulk gold is implemented across the whole work, with an elastic modulus of 81 GPa and a Poisson's ratio of 0.42, and the yield strength is 500 MPa without work hardening [7,15]. This arbitrarily chosen ligament strength corresponds to an average ligament diameter of approximately 200 nm [2], i.e., $r_0 = 100$ nm and $l = 400$ nm for a cylindrical ligament.

Table 1 lists the computational times for both the beam and solid models. The beam model shows a significant computational advantage over the solid model of approximately 3 orders of magnitude. Although the computational cost of the solid model could still be affordable in this single ligament analysis, the situation is completely different for the case of RVE simulations that contain thousands of ligaments resulting in a very high computational cost. The application of the beam model for NPG modelling is therefore vital for carrying out parametric studies and analyzing structure-property relationships. The current single ligament analysis provides an assessment of the accuracy level that the beam model could reach and has outstanding computational efficiency.

2.2. Results and discussion

The stiffness with respect to the three deformation modes, bending stiffness k_b, torsion stiffness k_t, and compression stiffness k_c, are calculated using Eqs. (4)–(6), respectively, where F_b, M_t and F_c are the resulting reaction forces for the bending, torque, and reaction forces for the compression of the ligament, respectively:

$$k_b = \frac{F_b}{w} \tag{4}$$

$$k_t = \frac{M_t}{\theta} \tag{5}$$

$$k_c = \frac{F_c}{v} \tag{6}$$

Fig. 3 shows the normalized stiffness results of both the beam (white marker) and solid models (black marker) for the three fundamental deformation modes (S.L. Bend, S.L. Torq, and S.L. Comp are the abbreviated terms for single ligament bending, torsion, and compression, respectively). All the stiffness results obtained for the different ligament shapes were normalized by the results from the cylindrical shape that serves as a reference (k_{b0}, k_{t0}, k_{c0} for bending, torsion and compression, respectively). It can be found that the two models show an almost symmetrical pattern in a single log plot: the center peak is near $r_{mid}/r_{end} = 1$ with concave ($r_{mid}/r_{end} < 1$) and convex ($r_{mid}/r_{end} > 1$) shapes located to the left and right sides of the peak, respectively.

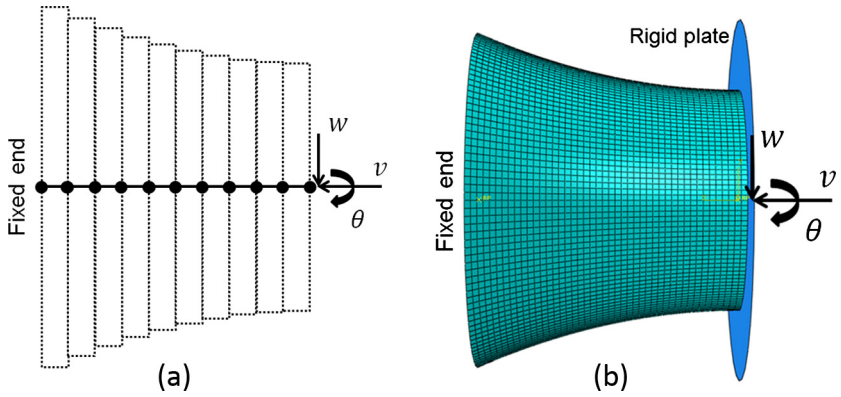

Fig. 2. An example of a ligament shape ($r_{mid}/r_{end} \approx 0.66$) for (a) beam model; (b) solid model; with load applications in the ligament center (with radius r_{mid}) and fixed boundary at the ligament end (with radius r_{end}).

Table 1
Computational cost of the single ligament analysis and estimation for an RVE analysis.

Model	CPU time for single ligament [h]	Estimated CPU time for RVE [h]
Beam	$1.4 \cdot 10^{-3}$–$2.8 \cdot 10^{-3}$	0.33–0.67
Solid	1.1–1.7	200–300

With respect to bending (Fig. 3a), the maximum stiffness is reached for the concave shape of $r_{mid}/r_{end} \approx 0.66$, which is close to the center line and approximately 1.25 and 1.1 times larger than the cylindrical ligament ($r_{mid}/r_{end} = 1$) for the solid and beam models, respectively. For this loading case, the maximum deviation of −12% is located at the peak, i.e., the beam model is more compliant compared to the solid model. In contrast, the results from the two other deformation modes (Fig. 3b and c) both reach their maximum stiffness for the cylindrical ligament. Deviations between the beam and solid models are negligible for torsion independent of the ligament shape and for compression of the concave ligaments. However, the convex ligaments under compression loading show an increasing overestimation of the stiffness by the beam model.

For the cases of compression and torsion, it can be concluded from Fig. 3 that a lower shape variation and deviation from the cylindrical shape leads to a stiffer mechanical response. For these two loading cases it is unimportant where the small cross section

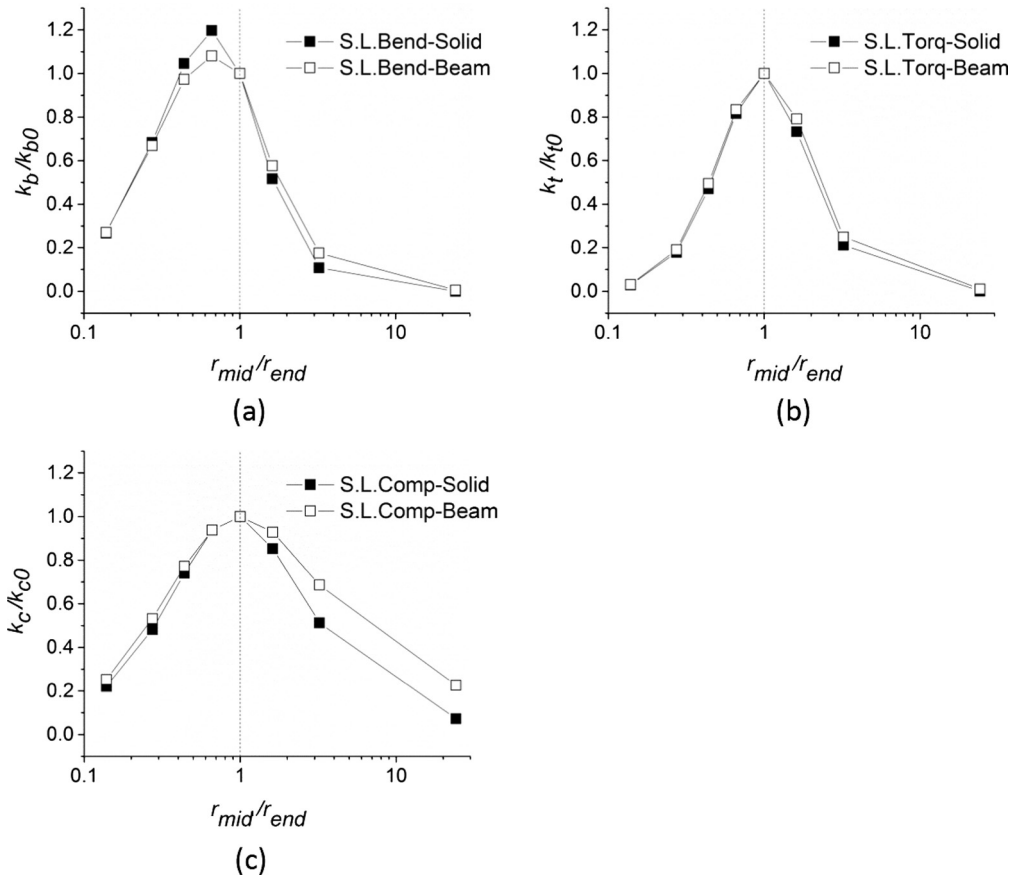

Fig. 3. Comparison between beam and solid models for the normalized stiffness results with respect to ligament shape variations in (a) bending; (b) torsion; (c) compression.

is located. It weakens the ligament stiffness in the same way everywhere, independent of whether it is at the ligament end or in the mid-section. Additionally, both appear symmetric around $r_{mid}/r_{end} = 1$, which can be distinguished by the width of their distribution: torsion shows a sharp peak, while compression results in a much broader distribution.

On the other hand, bending involves not only the moment of inertia but also the lever of load application, which causes asymmetry in the bending mode. That is, a slightly concave shape possesses maximum stiffness among all shape variations, which leads to its bending resistance being the strongest.

The agreement between the results from the beam and solid models indicates that it would be an applicable step to construct an RVE using beam elements only; 6% of the average deviation between these two models can be observed against the beam results, assuming there is an equal distribution of ligament shapes. This is well below the uncertainties and deviations between the models and the experimental data (see, e.g., [15]) and can be considered to be negligible. However, concerning the results shown in Fig. 3c, one critical question remaining for the RVE analysis is determining the relative contribution of compression deformation compared to bending and torsion. If compression turns out to be significant, using convex ligament shapes would lead to a systematic overestimation of the RVE's stiffness. In this case, it would be an important task to determine the probability distribution, e.g., from 3D FIB tomography data, particularly with regard to the occurrence of convex ligament shapes with larger r_{mid}/r_{end} values.

Using the observations and conclusions detailed above, further questions are raised to be answered in the next section. Could the characteristics of the single ligament behavior in different geometries be transferred to RVEs? What is the possible additional effect brought by network-construction (structural parameter) of the RVE to the relationship between the ligament geometry and the mechanical responses demonstrated in the current section?

In addition, the effect of the geometry on the yield strength has not yet been investigated. For compression and torsion, one can assume linearity until the yield stress is reached. However, the location and load level where plastic yield initiates in bending and mixed loading scenarios may not be represented simply by a linear dependency of the ligament stiffness. The resulting question is how well the single ligament results correlate with the macroscopic yield strength of a randomized RVE that contains a homogenized response of many ligaments as well as a mixture of the three load cases.

3. RVE analysis

In this section, the ligament shapes from Section 2 with an aspect ratio of $r_0/l = 0.25$ are implemented to construct RVEs. Additionally, two more cases using aspect ratios of $r_0/l = 0.35$ and 0.5 are also examined for broadening the range of RVE analyses. The RVE modelling approach in the current study is based on the beam model proposed in [7] and further refined in [15], where detailed information on the numerical modelling can be found.

3.1. Ordered RVE

To study the structural influences from a single ligament on the macroscopic behavior, the RVE is periodically constructed as a diamond lattice network [7] by unit cells ($A = 0$). The parameter of the unit cell size a is defined in [7] to characterize its structure (see Appendix A.1 of [7]). Three extreme examples with an aspect ratio of $r_0/l = 0.25$ are presented in Fig. 4a–c for a concave ligament RVE ($r_{mid}/r_{end} = 0.14$), cylindrical ligament RVE ($r_{mid}/r_{end} = 1$), and convex ligament RVE ($r_{mid}/r_{end} = 24.24$), respectively.

Table 2 defines the parameter range for the simulation runs. All ligament shapes (variations of r_{mid}/r_{end}) for the same r_0/l ratio possess the same material volume, which is equal to the volume of its corresponding cylindrical shape ligament ($r_{mid}/r_{end} = 1$). This ensures a constant material volume in the RVEs for the same r_0/l ratio. The different RVEs are loaded with the same compression deformation on the top surface. In Table 2, the variation of nr_0 applied to different r_0/l ligament groups leads to different ranges of r_{mid}/r_{end}, which is due to the fact that r_{mid}/r_{end} needs to be constrained to realistic geometries. Visual inspections of SEM images [10,22,28] encourage using a range of $r_{mid}/r_{end} = 0.3$ to 3 to describe the ligament shapes To make the analysis more comprehensive, ligament geometries outside of this range are also covered in the analyses but have fewer data points, as shown in Fig. 5.

Fig. 5a and b shows the results of the macroscopic Young's modulus (E) and yield strength (σ_y), respectively, for the perfectly ordered ligament network. As shown in Fig. 5a, three curves of different r_0/l ratios are constructed as a function of the ligament shape variations, parametrized via r_{mid}/r_{end}. E increases as expected with the r_0/l ratio that relates to the solid fraction φ. For a constant solid fraction, i.e., $r_0/l = const.$, varying the ligament shape shows the same effect on the stiffness of the RVE as is found for the single ligament under bending: the concave ligament with a shape close to the cylindrical shape leads to the highest value for E. Interestingly, for the yield strength σ_y in Fig. 5b, the peak value is at the

Table 2
Definition of the ranges of the r_0/l ratio and the shape variations r_{mid}/r_{end} of ordered RVEs for the numerical simulation runs.

r_0/l [–]	Range of $n \cdot r_0$ [–]	Range of r_{mid}/r_{end} [–]
0.5	[−0.87, 0.87]	[0.44, 3.23]
0.35	[−0.61, 0.61]	[0.29, 12.82]
0.25	[−0.32, 0.43]	[0.14, 24.24]

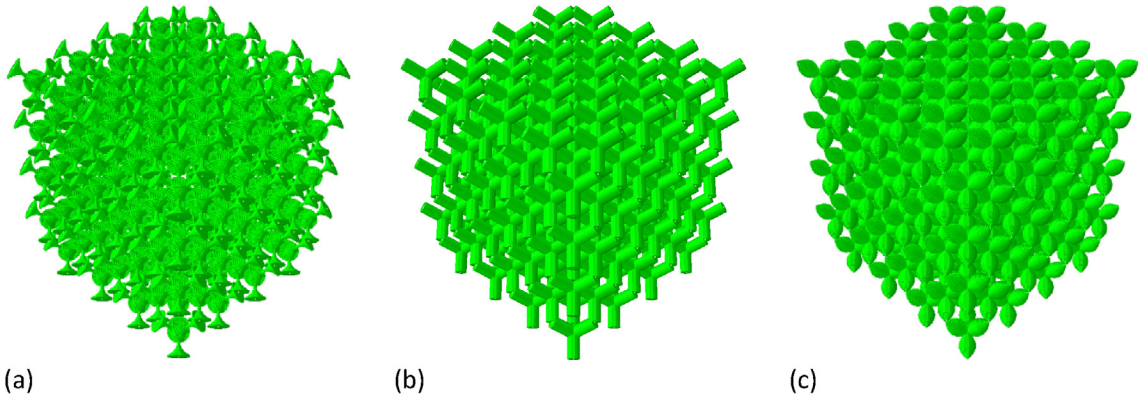

Fig. 4. Three examples of RVEs characterized by (a) concave ligament shape; (b) cylindrical ligament shape; and (c) convex ligament shape.

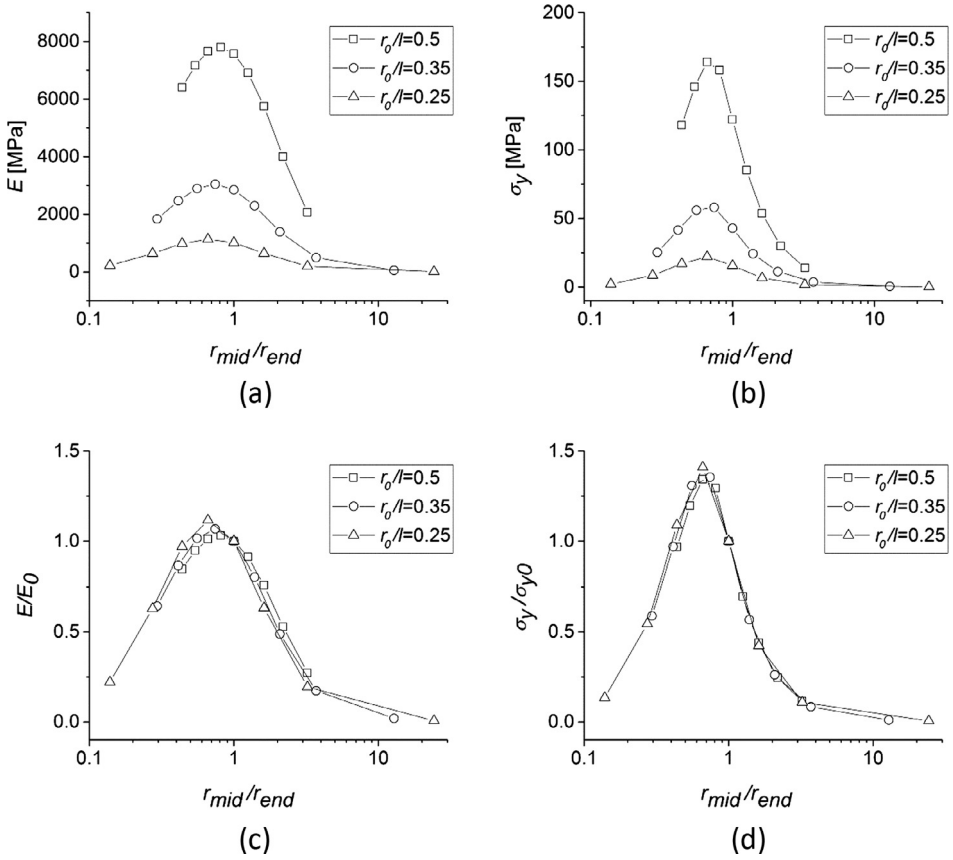

Fig. 5. Dependence of the macroscopic mechanical properties of the RVE on ligament shape r_{mid}/r_{end} for different r_0/l ratios. (a) Young's modulus E; (b) yield stress σ_y; (c) normalized macroscopic modulus; (d) normalized yield strength.

same value of $r_{mid}/r_{end} \approx 0.7$, but the distribution appears to be sharper than that of the Young's modulus.

In Fig. 5c and d, the results of E and σ_y for each of these three curves are normalized by the results of E_0 and σ_{y_0}, respectively. E_0 and σ_{y_0} are the Young's modulus and the yield strength of the corresponding cylindrical ligament RVEs ($r_{mid}/r_{end} = 1$), respectively. It is found that this normalization strategy leads to the converging of the E and σ_y results for different r_0/l ratios. The converged curves describe the relationship between the ligament geometry/network construction and the mechanical response of the RVE, where the effect of r_0/l (the material volume) is conveniently eliminated. This means that the very same network structure with cylindrical ligaments provides a common quantitative reference. The remaining deviations within the investigated range of the ligament aspect ratio are within 5% for the Young's modulus and 3% for the yield strength.

Two critical points can be derived from these results, which will form the basis for the next section. First, the ordered diamond network adds no significant effects on the normalized results of the macroscopic stiffness compared to the various shaped single ligament analysis. In other words, the ligament geometrical parameters still dominate the mechanical behavior of the ordered RVEs. This suggests that the modelling of a single ligament is a proper approach for describing the mechanical behavior as well as for the possible mixed loading induced by the deformation of the ligament network, at least with regard to the stiffness.

Second, the effects introduced by the aspect ratio of the ligament, r_0/l, can be eliminated by normalizing the results for both stiffness and strength with the results from the cylindrical ligament network. This includes the important effect of the solid fraction, as it has a one-to-one relationship with r_0/l. It can be concluded that the findings based on cylindrical ligaments from the previous work [7,15] serve as a valid reference at $r_{mid}/r_{end} = 1$ for the generalized case with an arbitrary ligament shape with $r_{mid}/r_{end} \neq 1$.

3.2. Randomized RVE

As originally stated in [31], the randomization of the structure plays a significant role in three-dimensional open-cell solids. This motivates further analyses by adding another structural parameter, A, that governs the severity of the nodal disorder for the beam model, as proposed in [7,15]. The randomization parameter A is related to the unit cell size a and determines the amplitude of a ligament connecting node's random shifts in space. In the current section, 23% and 40% of a are applied as magnitudes for the random shifting of the connecting nodes ($A = 0.23$ and 0.4, respectively). These selections are based on the investigation conducted in [15], where it is stated that $A = 0.4$ might be the maximum possible randomization, while $A = 0.23$ was found to be a proper randomization level that fit the measured ν_E best. Table 3 summarizes the parameter ranges for the simulation runs with randomized RVEs.

Table 3
Parameter ranges for the numerical simulation runs of RVEs with respect to nodal randomization levels, r_0/l ratio, and shape variations.

A [–]	r_0/l [–]	Range of r_{mid}/r_{end} [–]
0.23, 0.4	0.5	[0.44, 3.23]
0.23, 0.4	0.35	[0.29, 12.82]
0.23, 0.4	0.25	[0.14, 24.24]

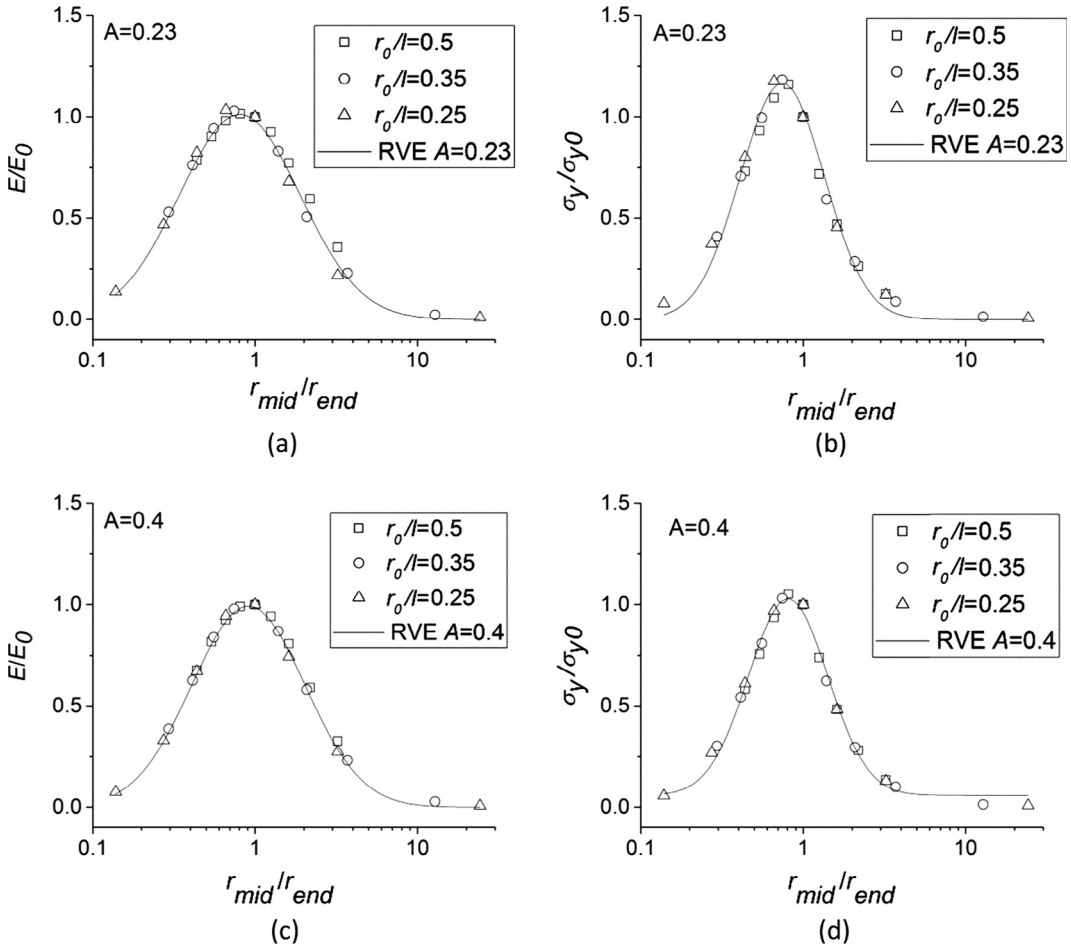

Fig. 6. Dependence of the macroscopic mechanical properties on the ligament shape r_{mid}/r_{end} for different r_0/l ratios. The markers represent the single ligament results of (a) normalized Young's modulus for $A = 0.23$; (b) normalized yield stress for $A = 0.23$; (c) normalized Young's modulus for $A = 0.4$; (d) normalized yield stress for $A = 0.4$.

Table 4
Parameters of the log-normal Eq. (7) fit to the normalized macroscopic modulus and yield strength of RVE.

Result normalization	A	ρ_1	ρ_2	ρ_3
$\frac{E}{E_0}$	0	2.52	0.89	1.59
	0.23	2.52	0.86	1.68
	0.4	2.51	0.80	1.73
$\frac{\sigma}{\sigma_0}$	0	1.40	0.57	0.90
	0.23	1.55	0.60	1.06
	0.4	1.30	0.56	1.11

The normalized results (of E and σ_y) for the two randomized networks $A = 0.23$ and $A = 0.4$ are shown in Fig. 6a–d, respectively. The comparison between Fig. 6 and Fig. 5 for the disordered and ordered RVE results shows that highly similar patterns in the RVE mechanical response can be obtained across different levels of randomization. The peak of the mechanical stiffness is again slightly below $r_{mid}/r_{end} = 1$, representing the cylindrical ligament shape.

For a better comparison and for further discussion, all the results are brought together in a single plot. To this end, the log-normal fitting function is used and represented with Eq. (7), where ρ, ρ_1, ρ_2, and ρ_3 are the ratio of r_{mid}/r_{end}, area, log standard deviation, and mean value, respectively; p and p_0 represent the macroscopic property for a given value of $\rho = r_{mid}/r_{end}$ (i.e., the result of E or σ_y) and the corresponding value for the cylindrical ligament (i.e., E_0 or σ_{y_0}), respectively. The parameters of the log-normal function, Eq. (7), for the normalized macroscopic modulus and the yield strength of $A = 0$, 0.23 and 0.4 are listed in Table 4. The coefficient of determination R^2 is in the range of 95–100% for all cases. The quality of the fits is demonstrated by the continuous curves in Fig. 6.

$$\frac{p}{p_0} = \frac{\rho_1}{\sqrt{2\pi}\cdot\rho\cdot\rho_2}\cdot e^{-\frac{(\ln\rho-\ln\rho_3)^2}{2\rho_2^2}} \tag{7}$$

For a direct comparison, in Fig. 7a, the fitting functions of RVE with $A = 0$, 0.23 and 0.4 for the macroscopic modulus (colored lines[1]) are plotted together with the single ligament normalized stiffness results from Fig. 3 (scatter lines). It can be seen from the comparison of the three continuous curves that the macroscopic Young's modulus decreases with increasing A only for $r_{mid}/r_{end} < 1$. For $r_{mid}/r_{end} > 1$, the effect of the randomization is comparably low. This can be understood from the concentration of the elastic deformation in the ligament ends in the vicinity of the nodes. The thicker the middle section is, the stiffer the ligaments remain, so that ligament-to-ligament variations in curvature and length have no noticeable effect.

The bending and torsion results for the single ligament seem to be highly correlated to the results from RVE for $A = 0$ and $A = 0.4$, respectively (see Fig. 7a). In other words, the mechanical characteristics of bending and torsion of individual ligaments govern

[1] For interpretation of color in Figs. 7 and 8a–c, the reader is referred to the web version of this article.

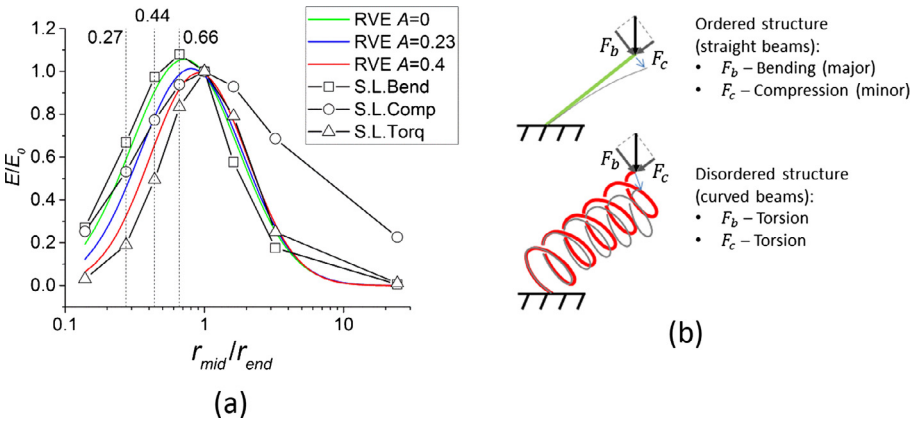

Fig. 7. (a) Comparison between the normalized E fitting functions of various randomization levels and single ligament normalized stiffness of bending, compression and torsion for RVE; (b) idealized models for extreme cases of perfectly ordered and ultimately disordered ligament network structures explaining the shift of the deformation mechanism from mainly bending to mainly torsion.

the deformation mechanisms of RVE during macroscopic compression deformation, depending on the degree of disorder. This hypothesis is supported by the shifting of the peak from $r_{mid}/r_{end} = 0.66$ to 1 and the narrowing of the distribution that is characteristic for torsion deformation, indicating that with increasing disorder, the deformation mode shifts from bending towards torsion. If we consider that each of these deformation modes are responsible for a certain percentage of the total deformation of the RVE, the contribution of bending would be dominant for $A = 0$. With increasing A, the proportion of bending would decrease, while that of torsion would increase.

The shift in the deformation mechanism can be intuitively understood by imagining the deformation of a straight beam and a spiral spring, as shown in Fig. 7b, where the latter is known as a mechanical element that mainly undergoes torsion deformation. Thus, the two models represent the extreme cases of a perfectly ordered and an ultimately disordered ligament network structure, illustrating why the patterns shown in Fig. 7a are mainly governed by the two deformation modes of bending and torsion.

On the other hand, the compression mode of the single ligament with its broad distribution is clearly the least relevant mechanism, and in view of the proposed spiral spring model shown in Fig. 7b, of no relevance for disordered network structures. This spiral spring model also explains the origin of the low degree of lateral expansion that is observed during compression of NPG [2,22]. This effect was successfully reproduced by tuning the degree of randomization of the ligament network [7,15], but until now, the underlying deformation mechanism remained unexplained.

Although bending is suggested to be the most dominant deformation in NPG compression by [7,18,19,23], our findings show that the effect of torsion is similarly important and should also be considered using nodal randomization. The macroscopic mechanical response of an RVE is the result of a mixture of these two fundamental deformation modes, which depends on the degree of randomization in the networking structure and the predominant ligament geometries.

Fig. 8 statistically underpins the previous hypothesis. To construct Fig. 8a–c, histograms of the bending moment, torque and compression force from all elements in the RVEs for $r_{mid}/r_{end} \approx 0.66$ ligament shape are collected under pure elastic deformation. The results of the bending moment M_b and torque M_t are then normalized by the product of the corresponding macroscopic reaction force of the RVE, F_{RVE}, and l; in addition, the data of the compression force are normalized by F_{RVE}. This approach cancels out the effect from the randomization on the stiffness of the RVE, providing dimensionless quantities for the quantitative comparison across RVEs with different randomization levels. For the special case of a perfectly ordered ($A = 0$) ligament network, the histogram of the bending moment in Fig. 8a shows a wavy pattern that possesses ten peaks. This is a result of the discretization of the ligaments with 20 elements (as introduced in Section 2.1.1). Each element has a certain distance to the next connecting node that, when multiplied by the bending force applied on each ligament end, yields the local bending moment. Due to the symmetry of the ordered structure, the resulting ten values for each half ligament (in the perfect structure all the ligaments are loaded in the same way) are reflected in the ten peaks, as shown in Fig. 8a.

With the increase of the nodal randomization level from 0 to 0.4, there are three aspects to note with regard to the deformation mechanism on the change in bending (Fig. 8a). First, the number of elements with bending deformation equal to or close to zero increases significantly from 100 for $A = 0$ to 1600 for $A = 0.4$. Second, the number of elements undergoing bending moments ranging from (not including) 0–0.0075, showing a significant reduction. Third, the number of elements undergoing larger bending moments ranging from 0.0075 to 0.015 increases but remains small.

On the other hand, it is obvious that torsion deformation increases with A, as shown in Fig. 8b. The number of ligaments with zero torsion abruptly decreases from 6000 for $A = 0$ to 1300 for $A = 0.4$, and this is accompanied by the increase in the range of the normalized torsion moment from approximately [−0.001, 0.001] to [−0.007 to 0.007]. These changes are caused by the ligament shape and curvature changes with respect to the increase in the randomization level.

As discussed in previous paragraphs, the compression is the least relevant factor for RVE macroscopic mechanical responses, and this is confirmed by Fig. 8c. It has some contribution in the ordered structure, which is visible in the form of a peak next to 0, but the peak is immediately shifted to zero normal force for disordered structures. For the diamond structure, the ratio of compression stress to bending stress is $\frac{\sigma_c}{\sigma_b} = \frac{1}{2\sqrt{2}} \frac{r_0}{l} \approx 0.35 \frac{r_0}{l}$ (also see Appendix A.2&3 in [7]), yielding a ratio of 0.09 for a typical ligament geometry of $r_0/l = 0.25$. Therefore, the contribution of compressive stress is slightly below 10% for the perfectly ordered structure and rapidly decreases with increasing degree of disorder. In conclusion, there are no issues concerning an overestimation of the macroscopic stiffness due to compression deformation of convex ligaments, as raised in the single ligament analysis in

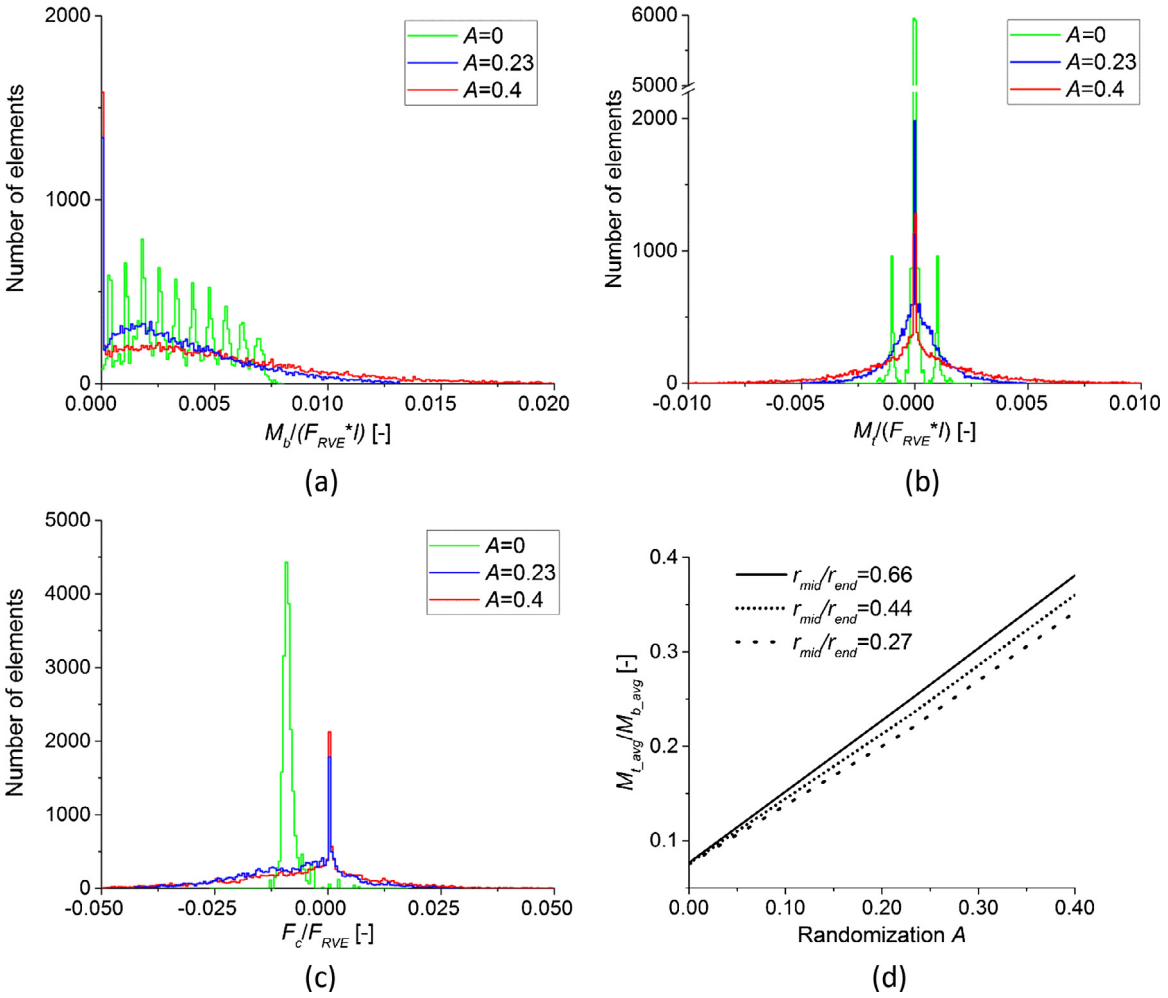

Fig. 8. Histograms showing the number of elements for the given normalized sectional moments and forces for three different randomization levels for (a) element bending, (b) torsion, and (c) uniaxial forces (mostly compression); (d) ratios of the averaged torques to bending moments for different ligament shapes.

Section 2.2, particularly when dealing with disordered ligament networks.

Up to now, the change for each of the fundamental deformations during RVE compression was analyzed; however, a clearer picture needs to be drawn to reveal the relationship between the fundamental deformation modes and RVE deformation with randomization. To this end, data from Fig. 8a and b are used to compute the ratio of the averaged torque to the averaged bending moment (M_{t_avg} and M_{b_avg}, respectively) over all elements in the RVE. The results are shown in Fig. 8d for RVEs of ligament shapes of $r_{mid}/r_{end} \approx 0.66, 0.44$ and 0.27. The choice of these geometries was motivated from the vertical lines inserted in Fig. 7a. The effect of randomization is clearly visible for concave shapes, while the effect vanishes for convex ligaments with $r_{mid}/r_{end} > 1$. Fig. 8d confirms that bending is the dominant deformation for $A = 0$. However, its influence decreases with increasing A. On the other hand, torsion contributes only a little for $A = 0$, but its contribution increases linearly with increasing disorder. As the randomization level reaches $A = 0.23$, the average ratios of torsion to bending are already within the same order of magnitude. The ratio approaches approximately 40% for $A = 0.4$. Furthermore, the ratio of torsion to bending is nearly independent of ligament shape r_{mid}/r_{end}. Fig. 8d quantitatively underpins the hypothesis deduced from Fig. 7 that bending and torsion govern the deformation characteristics of a nanoporous metal under macroscopic compression.

4. Conclusions

The paper provides new insights to the numerical modelling of nanoporous metals with respect to fundamental deformation mechanisms. The influences of the geometric parameters of the ligaments and randomization of the ligament network on the macroscopic mechanical response of an RVE are systematically analyzed and studied.

In the analysis of single ligaments, the applicability of the beam model is validated by a solid model in terms of three fundamental deformations, i.e., bending, torsion, and compression, for aspect ratios of ligament radius to ligament length of up to 0.5. The ligament shape has a strong effect on the stiffness and strength of the ligament. For torsion and compression, the cylindrical ligament reaches the maximum values, while the optimum ligament shape for bending is slightly concave. A significant deviation between the beam and solid models was found only for convex ligament shapes under compression loading. The RVE analysis showed that compression can be neglected as a deformation mechanism within the ligament network.

On the level of the RVE, it was concluded that the macroscopic mechanical response of the RVE is controlled by the ligament geometries comparable to the single ligament analysis. The findings based on cylindrical ligaments from previous work can be used as a common reference for the generalized cases with arbi-

trary ligament shapes. Moreover, the characteristics of the fundamental deformation mechanisms obtained for the single ligament were used for analyzing the deformation mechanisms in the RVE.

One key finding was that with increasing degree of randomization, the main deformation mechanism changes from bending to a mixed mode of deformation governed by bending and torsion. A simple spiral spring model was proposed that intuitively explains this effect and explains the low degree of lateral expansion that is observed during the compression of nanoporous gold.

Acknowledgments

Support was provided by Deutsche Forschungsgemeinschaft within SFB 986 "M3", project B4. Fruitful discussions with E.T. Lilleodden, J. Weissmüller, M. Ziehmer and Kaixiong Hu, as well as the support from B. Roschning in providing the Python code for RVE modelling, are gratefully acknowledged.

References

[1] R. Li, K. Sieradzki, Ductile-brittle transition in random porous Au, Phys. Rev. Lett. 68 (8) (1992) 1168.
[2] J. Weissmüller et al., Nanoporous metals by alloy corrosion: formation and mechanical properties, MRS Bull. 34 (08) (2009) 577–586.
[3] Y. Ding, M. Chen, Nanoporous metals for catalytic and optical applications, MRS Bull. 34 (08) (2009) 569–576.
[4] D. Kramer, R.N. Viswanath, J. Weissmüller, Surface-stress induced macroscopic bending of nanoporous gold cantilevers, Nano Letters 4 (5) (2004) 793–796.
[5] C. Stenner et al., Piezoelectric gold: strong charge-load response in a metal-based hybrid nanomaterial, Adv. Funct. Mater. (2016).
[6] L. Lührs et al., Elastic and plastic Poisson's ratios of nanoporous gold, Scr. Mater. 110 (2016) 65–69.
[7] N. Huber et al., Scaling laws of nanoporous metals under uniaxial compression, Acta Mater. 67 (2014) 252–265.
[8] P. Onck, Scale effects in cellular metals, MRS Bull. 28 (04) (2003) 279–283.
[9] J. Biener et al., Size effects on the mechanical behavior of nanoporous Au, Nano Letters 6 (10) (2006) 2379–2382.
[10] A. Hodge et al., Scaling equation for yield strength of nanoporous open-cell foams, Acta Mater. 55 (4) (2007) 1343–1349.
[11] J. Diao, K. Gall, M.L. Dunn, Surface-stress-induced phase transformation in metal nanowires, Nat. Mater. 2 (10) (2003) 656–660.
[12] K. Gall, J. Diao, M.L. Dunn, The strength of gold nanowires, Nano Letters 4 (12) (2004) 2431–2436.
[13] B. Wu, A. Heidelberg, J.J. Boland, Mechanical properties of ultrahigh-strength gold nanowires, Nat. Mater. 4 (7) (2005) 525–529.
[14] C.A. Volkert, E.T. Lilleodden, Size effects in the deformation of sub-micron Au columns, Phil. Mag. 86 (33–35) (2006) 5567–5579.
[15] B. Roschning, N. Huber, Scaling laws of nanoporous gold under uniaxial compression: effects of structural disorder on the solid fraction, elastic Poisson's ratio, Young's modulus and yield strength, J. Mech. Phys. Solids 92 (2016) 55–71.
[16] X.-Q. Feng et al., Surface effects on the elastic modulus of nanoporous materials, Appl. Phys. Lett. 94 (1) (2009) 011916.
[17] S. Bargmann et al., Materials based design of structures: computational modeling of the mechanical behavior of gold-polymer nanocomposites, Mech. Mater. 94 (2016) 53–65.
[18] G. Pia, F. Delogu, Nanoporous Au: statistical analysis of morphological features and evaluation of their influence on the elastic deformation behavior by phenomenological modeling, Acta Mater. 85 (2015) 250–260.
[19] G. Pia, F. Delogu, A phenomenological approach to yield strength in nanoporous metal foams, Scr. Mater. 103 (2015) 26–29.
[20] G. Pia, F. Delogu, Mechanical behavior of nanoporous Au with fine ligaments, Chem. Phys. Lett. 635 (2015) 35–39.
[21] R. Liu, A. Antoniou, A relationship between the geometrical structure of a nanoporous metal foam and its modulus, Acta Mater. 61 (7) (2013) 2390–2402.
[22] H.-J. Jin et al., Deforming nanoporous metal: role of lattice coherency, Acta Mater. 57 (9) (2009) 2665–2672.
[23] L.J. Gibson, M.F. Ashby, The mechanics of three-dimensional cellular materials, in: Proceedings of the Royal Society of London A: Mathematical, Physical and Engineering Sciences, The Royal Society, 1982.
[24] K. Wang et al., Nanoporous-gold-based composites: toward tensile ductility, NPG Asia Mater. 7 (6) (2015) e187.
[25] X.-Y. Sun et al., Mechanical properties and scaling laws of nanoporous gold, J. Appl. Phys. 113 (2) (2013) 023505.
[26] Abaqus Users Manual Version 6.14-1. Dassault Systémes Simulia Corp., Providence, RI.
[27] W.-Y. Jang, A.M. Kraynik, S. Kyriakides, On the microstructure of open-cell foams and its effect on elastic properties, Int. J. Solids Struct. 45 (7–8) (2008) 1845–1875.
[28] K. Hu, et al., Nanoporous gold: 3D structure analyses of RVEs and their implications on scaling relations of mechanical behavior. Philosophical Magazine Accepted, 2016.
[29] L.J. Gibson, M.F. Ashby, Cellular Solids: Structure and Properties, Cambridge University Press, 1997.
[30] H.-J. Jin, J. Weissmüller, A material with electrically tunable strength and flow stress, Science 332 (6034) (2011) 1179–1182.
[31] A. Roberts, E.J. Garboczi, Elastic properties of model random three-dimensional open-cell solids, J. Mech. Phys. Solids 50 (1) (2002) 33–55.